International Communications in Heat and Mass Transfer 118 (2020) 104883

Contents lists available at ScienceDirect

International Communications in Heat and Mass Transfer

journal homepage: www.elsevier.com/locate/ichmt

Hydrodynamics and ferrite nanoparticles in hybrid nanofluid

Jing Yang[a], Zahra Abdelmalek[b,c,*], Noor Muhammad[d], M.T. Mustafa[e]

[a] School of Control and Computer Engineering, North China Electric Power University, Beijing 102206, China
[b] Institute of Research and Development, Duy Tan University, Da Nang 550000, Vietnam
[c] Faculty of Medicine, Duy Tan University, Da Nang 550000, Vietnam
[d] Department of Mathematics, Quaid-I-Azam University 45320, Islamabad 44000, Pakistan
[e] Department of Mathematics, Statistics and Physics, Qatar University, Doha 2713, Qatar

ARTICLE INFO

Keywords:
Fe_3O_4
$MnZnFe_2O_4$
H_2O
$C_2H_2F_4$

ABSTRACT

The solids have higher heat transfer rate comparative to fluids, thus, in the present article, two different ferrite nano-particles are suspended in two different base fluids to demonstrates its impacts on the friction drag and heat transfer. Ferrites nano-particles are used because of the existence of Curie temperature in these particles, a property that makes them distinct from other nano-particles. Distinct ferrites have different Curie temperature, this means that the presence of ferrite nano-particles in base fluids makes them efficient for heat transfer in ferromagnetic fluid flows. Thus, this article focuses to study two ferrites, i.e., Magnetite ferrite Fe_3O_4 and Manganese zinc ferrite $MnZnFe_2O_4$ with base fluids water H_2O and refrigerant-134A $C_2H_2F_4$. Heat transfer and friction drag are carried out for these hybridized ferrites nanoparticles in ferromagnetic nano-fluids. The higher velocity field is seen for the hybrid nanofluid $MnZnFe_2O_4$-Fe_3O_4-H_2O-$C_2H_2F_4$, whereas, the lowest velocity field is demonstrated for the nanofluid Fe_3O_4-H_2O.

1. Introduction

In continuum model, thermal motion of molecules plays an important role as it leads to exchange process, in which, the molecules migrate out of particles of fluid and are restored with molecules drifting in. This exchange process leads to the well-known properties of fluids termed as transport properties. From this point of view, viscosity in the momentum transport is the source of internal friction, whereas, thermal conductivity is the internal source of heat in the temperature equation, and diffusion is the internal source of mass distribution in the concentration equation. It is known from findings on the heat transfer and friction drag in area of dynamics that thermal conductivity is smaller in liquids and higher for solids [1–5]. Since increased thermal conductivity implies increased transfer of heat, so if solid (nano-size) particles are suspended in the liquids their heat transfer will rise [6–10].

Ferrites nano-particles ($1 - 100nmsized$) have higher thermal conductivity with the additional property of ferromagnetism. An important characteristic of ferrite is the well known property of Curie temperature, at which ferrite nanoparticles lose their magnetization. Different ferrites have different Curie temperatures [11–13]. These ferrites nanoparticles are useful in different industrial as well as technological and biological areas [14–20].

The property of Curie temperature makes the ferrites particles useful in electronics to evacuate heat and make them last longer. An example of effective application of these ferrites is their use in loudspeakers and Lenovo laptops. The transfer of heat in latest loudspeakers and Lenovo laptops is taking place through utilization of the magnetic fluid, which is made of base fluid with suspension of ferrite nanoparticles in it. When these devices become heated, the nearer placed magnetic fluid absorbs heat. The fluid contains ferrites which, when heated up, lose their magnetization because of Curie temperature and get back to cool places by magnetic dipole. This is how the heat transfer takes place in these electronics, which is a low cost and efficient way to transfer heat from electronics [21–25].

Keeping in mind the idea of transfer of heat in solids and liquids, this article investigates the hybrid nano-fluids. Two different types of ferrites nano-particles i.e., Fe_3O_4, $MnZnFe_2O_4$ with base fluids refrigerant-134A $C_2H_2F_4$ and water H_2O are analyzed. Because different ferrites have different Curie temperatures, their combination will make heat transfer efficiency in applications in electronics and other devices. The results of the study can also be applied in refrigerators for stabilizing the cooling rate in refrigerators.

2. Mathematical modeling

The geometric flowchart is displayed in Fig. 1. Flow of a viscous

* Corresponding author at: Institute of Research and Development, Duy Tan University, Da Nang 550000, Vietnam
E-mail address: zahraabdelmalek@duytan.edu.vn (Z. Abdelmalek).

https://doi.org/10.1016/j.icheatmasstransfer.2020.104883

Available online 22 September 2020

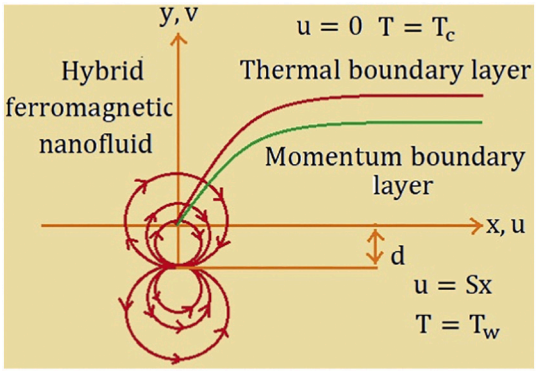

Fig. 1. Geometry of the flow.

Table 1
Thermo-physical properties for ferrites nano-particles.

	ρ (kg/m^3)	C_p (J/kgK)	k (W/mK)	Pr
H_2O	997	4179	0.613	6.9
$C_2H_2F_4$	1199.7	1432.0	0.0803	3.2
Fe_3O_4	5180	670	9.7	–
$MnZnFe_2O_4$	4700	1050	3.9	–

fluid is taken in such a way that in a single base fluid two different ferrites nano-particles are suspended. Two different types of fluids with hybrid nano-particles are synthesized. Initially, Fe_3O_4, $MnZnFe_2O_4$ ferrites are taken with the base fluid refrigerant-134A $C_2H_2F_4$, secondly, Fe_3O_4, $MnZnFe_2O_4$ ferrites are taken with the base fluid water H_2O. The flow of ferromagnetic fluid past a stretchable surface is incorporated. The ferrite nano-particles and base fluids are in thermal equilibrium. An external magnetic dipole is considered in the analysis. Equations for thermomechanical coupling are given in Eq. (1 − 3), whereas, the boundary conditions are given in Eq. (4) and (5). The thermo-physical properties of refrigerant-134A $C_2H_2F_4$, water H_2O, Fe_3O_4, and $MnZnFe_2O_4$ are given in Table 1. The volume fraction $\varphi_1 = 0.1$ of magnetite ferrite Fe_3O_4 nano-particles is suspended in the base fluid refrigerant-134A $C_2H_2F_4$ and water H_2O to make hybrid ferromagnetic nanofluid Fe_3O_4-$C_2H_2F_4$-H_2O. Thus, to get the targeted hybrid nanofluid, the volume fraction $\varphi_2 = 0.01$ of $MnZnFe_2O_4$ is added to Fe_3O_4-$C_2H_2F_4$-H_2O ferromagnetic nanofluid which forms the hybrid ferromagnetic nanofluid $MnZnFe_2O_4$-Fe_3O_4-$C_2H_2F_4$-H_2O. Fourier's law of heat conduction is utilized in the evaluation of heat flux. The equations of interest are

$$\frac{\partial u}{\partial x} + \frac{\partial v}{\partial y} = 0, \tag{1}$$

$$\rho_{hnf}\left(u\frac{\partial u}{\partial x} + v\frac{\partial u}{\partial y}\right) = -\frac{\partial P}{\partial x} + \mu_{hnf}\frac{\partial^2 u}{\partial y^2} + \mu_0 M\frac{\partial H}{\partial x}, \tag{2}$$

$$(\rho c_p)_{hnf}\left(u\frac{\partial T}{\partial x} + v\frac{\partial T}{\partial y}\right) + (\rho c_p)_{hnf}\mu_0 T\frac{\partial M}{\partial T}\left(u\frac{\partial H}{\partial x} + v\frac{\partial H}{\partial y}\right) = k_{hnf}\frac{\partial^2 T}{\partial y^2}. \tag{3}$$

Here (u,v) exemplify the components of velocity field along (x,y) respectively, μ_{hnf} demonstrates the dynamic viscosity of hybrid nanofluid, ρ_{hnf} displays density of hybrid nanofluid, P signify pressure, T symbolize the temperature, $(\rho c_p)_{hnf}$ represents the specific heat, whereas k_{hnf} indicates the thermal conductivity of hybrid nanofluid, magnetic field is demonstrated with H, and the respective magnetization is described by M. Boundary conditions are

$$u|_{y=0} = Sx, \qquad v|_{y=0} = 0, \qquad T|_{y=0} = T_w, \tag{4}$$

$$u|_{y\to\infty} = 0, \qquad T|_{y\to\infty} = T_c. \tag{5}$$

Table 2
Mathematical expressions for thermo-physical properties for ferrites nano-particles.

Properties	Fe_3O_4-H_2O
Density ρ	$\rho_{nf} = (1-\varphi)\rho_f + \varphi\rho_s$
Viscosity μ	$\mu_{nf} = \mu_f(1-\varphi)^{-25/10}$
Heat Capacity ρC_p	$(\rho c_p)_{nf} = (1-\varphi)(\rho c_p)_f + \varphi(\rho c_p)_s$
Thermal Conductivity k	$\frac{k_{nf}}{k_f} = \frac{2k_f + k_s - 2\varphi(k_f - k_s)}{2k_f + k_s + \varphi(k_f - k_s)}$
Properties	$MnZnFe_2O_4$-Fe_3O_4-$C_2H_2F_4$
Density ρ	$\rho_{hnf} = (1-\varphi_2)((1-\varphi_1)\rho_f + \varphi_1\rho_{s_1}) + \varphi_2\rho_{s_2}$
Viscosity μ	$\mu_{hnf} = \mu_f(1-\varphi_1)^{-25/10}(1-\varphi_2)^{-25/10}$
Heat Capacity ρC_p	$(\rho c_p)_{nf} = (1-\varphi_2)((1-\varphi_1)(\rho c_p)_f + \varphi_1(\rho c_p)_{s_1}) + \varphi_2(\rho c_p)_{s_2}$
Thermal Conductivity k	$\frac{k_{hnf}}{k_{bf}} = \frac{2k_{bf} + k_{s2} - 2\varphi_2(k_{bf} - k_{s2})}{2k_{bf} + k_{s2} + \varphi_2(k_{bf} - k_{s2})}$ $\frac{k_{bf}}{k_f} = \frac{2k_f + k_{s1} - 2\varphi_1(k_f - k_{s1})}{2k_f + k_{s1} + \varphi_1(k_f - k_{s1})}$
Properties	Fe_3O_4-$MnZnFe_2O_4$-H_2O
Density ρ	$\rho_{hnf} = (1-\varphi_2)((1-\varphi_1)\rho_f + \varphi_1\rho_{s_1}) + \varphi_2\rho_{s_2}$
Viscosity μ	$\mu_{hnf} = \mu_f(1-\varphi_1)^{-25/10}(1-\varphi_2)^{-25/10}$
Heat Capacity ρC_p	$(\rho c_p)_{nf} = (1-\varphi_2)((1-\varphi_1)(\rho c_p)_f + \varphi_1(\rho c_p)_{s_1}) + \varphi_2(\rho c_p)_{s_2}$
Thermal Conductivity k	$\frac{k_{hnf}}{k_{bf}} = \frac{2k_{bf} + k_{s2} - 2\varphi_2(k_{bf} - k_{s2})}{2k_{bf} + k_{s2} + \varphi_2(k_{bf} - k_{s2})}$ $\frac{k_{bf}}{k_f} = \frac{2k_f + k_{s1} - 2\varphi_1(k_f - k_{s1})}{2k_f + k_{s1} + \varphi_1(k_f - k_{s1})}$
Properties	$MnZnFe_2O_4$-Fe_3O_4-$C_2H_2F_4$-H_2O
Density ρ	$\rho_{hnf} = (1-\varphi_2)((1-\varphi_1)(\rho_{f_1} + \rho_{f_2}) + \varphi_1(\rho_{s_1} + \rho_{s_2})) + \varphi_2(\rho_{s_1} + \rho_{s_2})$
Viscosity μ	$\mu_{hnf} = (\mu_{f_1} + \mu_{f_2})(1-\varphi_1)^{-25/10}(1-\varphi_2)^{-25/10}$
Heat Capacity ρC_p	$(\rho c_p)_{hnf} = (1-\varphi_2)((1-\varphi_1)((\rho c_p)_{f_1} + (\rho c_p)_{f_2}) + \varphi_1((\rho c_p)_{s_1} + (\rho c_p)_{s_2})) + \varphi_2(\rho c_p)_{s_1} + (\rho c_p)_{s_2})$
Thermal Conductivity k	$\frac{k_{hnf}}{k_{bf_1} + k_{bf_2}} = \frac{2(k_{bf_1} + k_{bf_2}) + (k_{s1} + k_{s2}) - 2\varphi_2((k_{bf_1} + k_{bf_2}) - (k_{s1} + k_{s2}))}{2(k_{bf_1} + k_{bf_2}) + (k_{s1} + k_{s2}) + \varphi_2((k_{bf_1} + k_{bf_2}) - (k_{s1} + k_{s2}))}$ $\frac{k_{bf_1} + k_{bf_2}}{k_{f_1} + k_{f_2}} = \frac{2(k_{f_1} + k_{f_2}) + (k_{s1} + k_{s2}) - 2\varphi_1((k_{f_1} + k_{f_2}) - (k_{s1} + k_{s2}))}{2(k_{f_1} + k_{f_2}) + (k_{s1} + k_{s2}) + \varphi_1((k_{f_1} + k_{f_2}) - (k_{s1} + k_{s2}))}$

The first boundary condition for velocity field given in Eq. (4) describes stretching at the surface and S demonstrates the rate of stretching, where as T_c (Curie temperature) is defined far from the wall. The thermo-physical properties μ_{hnf}, ρ_{hnf}, $(\rho c_p)_{hnf}$, and k_{hnf} and their thermo-physical properties and mathematical expressions for hybrid ferromagnetic nanofluids are give in Tables 1 and 2.

2.1. Magnetic dipole

An external magnet is placed on vertical axis at a distance d below horizontal axis, this magnet induces magnetic field that attracts ferrite nano-particles below curie temperature. Heated particles above curie temperature are going far from magnet because of no magnetization, this leads to heat transfer in fluid flows because of magnetic dipole. The magnetic scalar potential function ρ for the magnetic diploe is defined as

$$\rho = \frac{\gamma_1}{2\pi}\frac{x}{x^2 + (y+d)^2}, \tag{6}$$

γ_1 demonstrates the magnetic field induction, by means of ρ the magnetic field H can be defined as

$$H = \sqrt{\left(\frac{\partial \rho}{\partial x}\right)^2 + \left(\frac{\partial \rho}{\partial y}\right)^2}, \tag{7}$$

the magnetization is the linear function of temperature, i.e.,

$$M = K_m(T - T_\infty), \tag{8}$$

here K_m signify the pyromagnetic coefficient, the geometry for the flow analysis in the present problem is given in Fig. 1.

2.2. Similarity analysis

The similarity transformation are used to reduce the system of partial differential equations equations given in Eqs. (1–3) along with boundary conditions given in Eqs. 4 and 5, are defined as

$$\psi(\eta,\xi)=\left(\frac{\mu_f}{\rho_f}\right)\eta f(\xi),$$
$$\theta(\eta,\xi)\equiv\frac{T_c-T}{T_c-T_w}=\theta_1(\xi)+\eta^2\theta_2(\xi), \tag{9}$$

the corresponding velocity components and dimensionless coordinates are

$$\xi=y\left(\frac{\rho_f S}{\mu_f}\right)^{\frac{1}{2}},\qquad \eta=x\left(\frac{\rho_f S}{\mu_f}\right)^{\frac{1}{2}},$$
$$u=\frac{\partial\psi}{\partial y}=Sxf'(\xi),\qquad v=-\frac{\partial\psi}{\partial x}=-(S\nu_f)^{\frac{1}{2}}f(\xi). \tag{10}$$

Making use of similarity transformation reduces the system of partial differential equations equations given in Eqs. (1–3) along with boundary conditions given in Eqs. 4 and 5 to the following form

$$\frac{1}{(1-\varphi_1)^{\frac{25}{10}}(1-\varphi_2)^{\frac{25}{10}}A_1}f'''-(f')^2+ff''-\frac{2\beta\theta_1}{A_1(\xi+\gamma)^4}=0, \tag{11}$$

$$\frac{k_{hnf}}{(k_{f_1}+k_{f_1})A_2}\theta_1''+Pr(f\theta_1'-2f'\theta_1)+\frac{2\lambda\beta f(\theta_1-\varepsilon)}{A_2(\xi+\gamma)^3}-\frac{4\lambda}{A_2}(f')^2=0, \tag{12}$$

$$\frac{k_{hnf}}{(k_{f_1}+k_{f_1})A_2}\theta_2''-Pr(4f'\theta_2-f\theta_2')+\frac{2\lambda\beta f\theta_2}{A_2(\xi+\gamma)^3}$$
$$-\frac{\lambda\beta(\theta_1-\varepsilon)}{(\xi+\gamma)^3}\left(\frac{2f'}{(\xi+\gamma)^4}+\frac{4f}{(\xi+\gamma)^5}\right)-\frac{\lambda}{A_2}(f'')^2=0, \tag{13}$$

$$f(\xi)=0,\quad f'(\xi)=1,\quad \theta_1(\xi)=1,\quad \theta_2(\xi)=0,\quad at\quad \xi=0,$$
$$f'(\xi)\to 0,\quad \theta_1(\xi)\to 0,\quad \theta_2(\xi)\to 0,\quad when\quad \xi\to\infty, \tag{14}$$

here A_1 and A_2 are defined bellow

$$A_1=(1-\varphi_2)\left((1-\varphi_1)+\varphi_1\frac{(\rho_{s_1}+\rho_{s_2})}{(\rho_{f_1}+\rho_{f_2})}\right)+\varphi_2\frac{(\rho_{s_1}+\rho_{s_2})}{(\rho_{f_1}+\rho_{f_2})},$$

$$A_2=(1-\varphi_2)\left((1-\varphi_1)+\varphi_1\frac{((\rho c_p)_{s_1}+(\rho c_p)_{s_2})}{((\rho c_p)_{f_1}+(\rho c_p)_{f_2})}\right)+\varphi_2\frac{((\rho c_p)_{s_1}+(\rho c_p)_{s_2})}{((\rho c_p)_{f_1}+(\rho c_p)_{f_2})}. \tag{15}$$

In system of nonlinear equation given above contains the parameters, β (Ferrohydrodynamic interaction), λ (Viscous dissipation), *Pr* (Prandtl number), and ε (Curie temperature). The mathematical expressions of these parameters are given as

$$\varepsilon=\frac{T_\infty}{T_c-T_w},\quad Pr=\frac{\nu_f}{\alpha_f},\quad \beta=\frac{\gamma_1}{2\pi}\frac{\mu_0K_m(T_c-T_w)\rho_f}{\mu_f^2},$$
$$\gamma=\sqrt{\frac{S\rho_f d^2}{\mu_f}},\quad \lambda=\frac{S\mu_f^2}{\rho_f K_m(T_c-T_w)}. \tag{16}$$

The friction drag and heat transfer rate for the under discussion problem are

$$C_f=\frac{\tau_w}{\frac{1}{2}\rho_{hnf}U_w^2},\qquad \tau_w=\mu_{hnf}\left.\frac{\partial u}{\partial y}\right|_{y=0},$$
$$Nu_x=\frac{xk_{hnf}}{(k_{f_1}+k_{f_2})(T_c-T_w)}\left.\frac{\partial T}{\partial y}\right|_{y=0}. \tag{17}$$

The friction drag and heat transfer rate take the final dimensionless form as

$$\frac{1}{2}Re_x^{\frac{1}{2}}C_f=\frac{1}{(1-\varphi_1)^{\frac{25}{10}}(1-\varphi_2)^{\frac{25}{10}}}f''(0),$$
$$Re_x^{-\frac{1}{2}}Nu_x=\frac{k_{hnf}}{(k_{f_1}+k_{f_2})}(\theta_1(0)+\eta^2\theta_2(0)). \tag{18}$$

Here Re_x demonstrated the Reynolds number that means the ratio of inertial forces to viscous forces, i.e., $Re_x=xU_w/\nu_f$, whereas, $\frac{1}{2}Re_x^{\frac{1}{2}}C_f$ and $Re_x^{-\frac{1}{2}}Nu_x$ describes the respective local skin friction and local Nusselt number.

Optimal Homotopy Analysis Method (Optimal HAM) [26,27] is used to solve the problem. Optimal HAM provides flexibility to choose auxiliary linear operators and initial guesses. For present flow problem, linear operators and initial guesses are

$$L_f(f)=\frac{d^3f}{d\xi^3}+\frac{d^2f}{d\xi^2},\ L_{\theta_1}(\theta_1)=\frac{d^2\theta_1}{d\xi^2}-\theta_1,\ L_{\theta_2}(\theta_2)=\frac{d^2\theta_2}{d\xi^2}-\theta_2,$$
$$f_0(\xi)=1-\exp(-\xi),\ \theta_{1_0}(\xi)=\exp(-\xi),\ \theta_{2_0}(\xi)=\xi\exp(-\xi). \tag{19}$$

Auxiliary parameters defined for the present problem are h_f, h_{θ_1}, and h_{θ_2}. These parameters play role in stabilizing convergence of series solution. The residual errors determined for the momentum and energy equations by means of following mathematical equations

$$\Delta_m^f=\int_0^1[\mathscr{R}_m^f(\xi,h_f)]^2d\xi,$$
$$\Delta_m^{\theta_1}=\int_0^1[\mathscr{R}_m^{\theta_1}(\xi,h_{\theta_1})]^2d\xi,$$
$$\Delta_m^{\theta_2}=\int_0^1[\mathscr{R}_m^{\theta_2}(\xi,h_{\theta_2})]^2d\xi. \tag{20}$$

The convergence for the optimal HAM is shown in Tables 3 and 4. $\Delta_m{}^t$ depicts the total residual error.

Error decay for order 12th is shown in Fig. 2, whereas the optimal convergence control parameter is depicted via total residual square error $\Delta_m{}^t$.

$$\Delta_m^t=\Delta_m^f+\Delta_m^{\theta_1}+\Delta_m^{\theta_2}. \tag{21}$$

3. Discussion

The mathematical analysis of ferrites particles, i.e., Fe_3O_4 and $MnZnFe_2O_4$ on the fluid flows of two different base fluids, i.e., water H_2O and refrigerant-134A $C_2H_2F_4$ is carried out in this section. Heat transfer is discussed for the flow analysis and results got for the ferromagnetic fluids along ferrites nanoparticles shown significant results displayed in the graphical results. Figs. 3 and 4 delineates the comparison of velocity and temperature fields in different hybrid nanofluids, i.e., $MnZnFe_2O_4$-Fe_3O_4-H_2O-$C_2H_2F_4$, Fe_3O_4-$MnZnFe_2O_4$-H_2O, $MnZnFe_2O_4$-Fe_3O_4-$C_2H_2F_4$ and a simple nanofluid Fe_3O_4-H_2O. Fig. 3

Table 3
Average residual square errors $\Delta_m{}^t$.

Order	h_f	h_{θ_1}	h_{θ_2}	$\Delta_m{}^t$
4	−0.07509	−0.50142	−0.80381	0.00010202
6	−0.20631	−0.59829	−0.83609	1.05490×10^{-06}
8	−0.40713	−0.60919	−0.94103	2.58202×10^{-11}
10	−0.89042	−0.82141	−0.95082	1.67025×10^{-16}
12	−1.30201	−0.90216	−1.10351	3.09961×10^{-20}

Table 4
Individual residual square errors Δ_m^f, $\Delta_m^{\theta_1}$, and $\Delta_m^{\theta_2}$ when $h_f = -1.30201$, $h_{\theta_1} = -0.90216$, and $h_{\theta_2} = -1.10351$.

Order	Δ_m^f	$\Delta_m^{\theta_1}$	$\Delta_m^{\theta_2}$
10	3.60921×10^{-13}	8.21009×10^{-09}	3.88319×10^{-05}
12	2.04402×10^{-17}	5.30218×10^{-12}	4.99004×10^{-06}
14	5.04165×10^{-19}	6.99043×10^{-16}	1.50993×10^{-09}
18	3.66903×10^{-22}	1.69032×10^{-19}	7.60427×10^{-16}
22	7.55198×10^{-23}	9.00312×10^{-22}	2.50941×10^{-22}

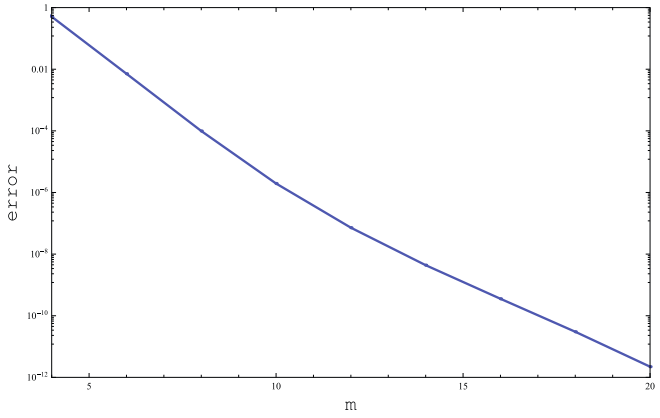

Fig. 2. Error decay for the 12th order approximation.

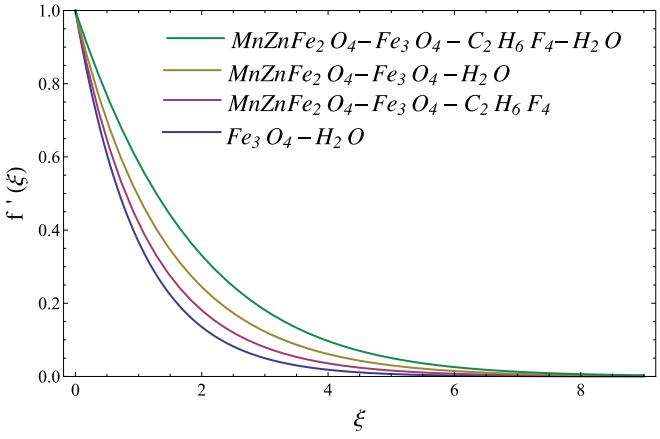

Fig. 3. Comparision of velocity field in hybrid ferromagnetic nanofluid.

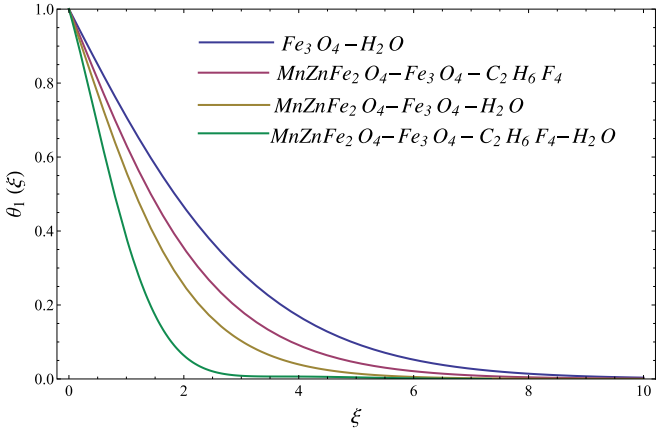

Fig. 4. Comparision of temperature field in hybrid ferromagnetic nanofluid.

reveals the comparison of axial velocity among different ferrites particles and base fluid. The higher velocity field is seen for the hybrid nanofluid $MnZnFe_2O_4$-Fe_3O_4-H_2O-$C_2H_2F_4$, whereas, the lowest velocity field is demonstrated for the nanofluid Fe_3O_4-H_2O revealed in Fig. 3. This means that the axial velocity has better performance in hybrid nanofluids, i.e., $MnZnFe_2O_4$-Fe_3O_4-H_2O-$C_2H_2F_4$, it is because that in hybrid nanofluid have different densities of base fluids and ferrites particles, which reduces the resistance between fluid layers and as a result, the velocity improves for hybrid nanofluids as compare to simple nanofluids. The presence of more ferrite particles in the different base fluid enhances the density of the resultant hybrid nanofluid which will affect the Curie temperature of the combined ferrites nanoparticles in the base fluid, it means that in electronics and other equipment hybrid nanofluids play better performance. Fig. 4 demonstrates the temperature field in the flow of hybrid nanofluids $MnZnFe_2O_4$-Fe_3O_4-H_2O-$C_2H_2F_4$, Fe_3O_4-$MnZnFe_2O_4$-H_2O, $MnZnFe_2O_4$-Fe_3O_4-$C_2H_2F_4$ and a simple nanofluid Fe_3O_4-H_2O. By Fig. 4 it seems that the temperature field declines in analyzing hybrid nanofluids, the higher reduction in temperature field is depicted for the $MnZnFe_2O_4$-Fe_3O_4-H_2O-$C_2H_2F_4$ hybrid nanofluid whereas the highest temperature field is demonstrated for the simple nanofluid Fe_3O_4-H_2O. The temperature field is lower for the hybrid nanofluid because of the presence of distinct ferrites particles with different thermal conductivities and heat capacities along with Curie temperature. Hybrid nanofluid makes heat transfer rate efficient because their thermal conductivity and heat capacity along Curie temperature is combination of base fluid water H_2O and refrigerant-134A $C_2H_2F_4$ and ferrites particles Fe_3O_4 and $MnZnFe_2O_4$. This means that $MnZnFe_2O_4$-Fe_3O_4-H_2O-$C_2H_2F_4$ hybrid nanofluid has the higher heat transfer rate, and simple nanofluid Fe_3O_4-H_2O has lowest heat transfer rate. Thus the fast reduction in temperature field is depicted for the $MnZnFe_2O_4$-Fe_3O_4-H_2O-$C_2H_2F_4$ hybrid nanofluid and the lowest reduction is analyzed for simple nanofluid Fe_3O_4-H_2O. Physically, making use of different ferrites particles makes the Curie temperature differ through which magnetization arises and as a result heating or cooling rates arise in the electronic devices, which means that hybrid nanofluids will be more efficient as compare to simple ferrofluids.

Figs. 5 and 6 demonstrate the velocity and temperature comparisons when base fluids are changed to study which base fluid performs better. Remember that the hybrid nanofluid is made in such a way that in a single base fluid two different ferrites nanoparticles were suspended and then the suspension is analyzed mathematically to study the performance of heat transfer in a resultant ferromagnetic hybrid nanofluid. These figures further show the impacts of β (Ferrohydrodynamic interaction) on the axial velocity and temperature field. Fig. 5 displays the influence of β (Ferrohydrodynamic interaction) on velocity field for base fluid water H_2O and refrigerant-134A $C_2H_2F_4$ and ferrites nanoparticles Fe_3O_4 and $MnZnFe_2O_4$. The figure shows that water H_2O has

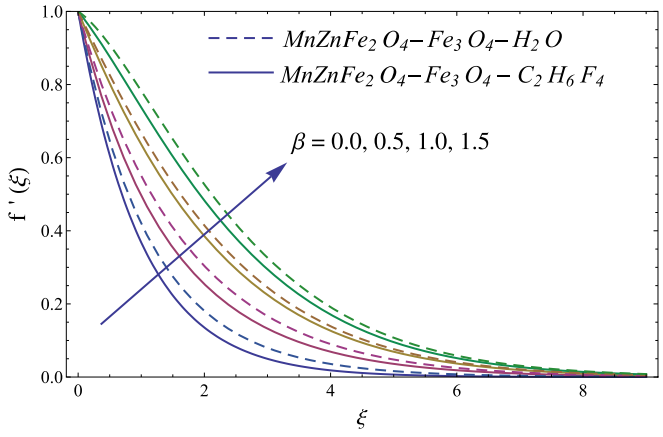

Fig. 5. Influence of β on axial velocity of hybrid ferromagnetic nanofluid.

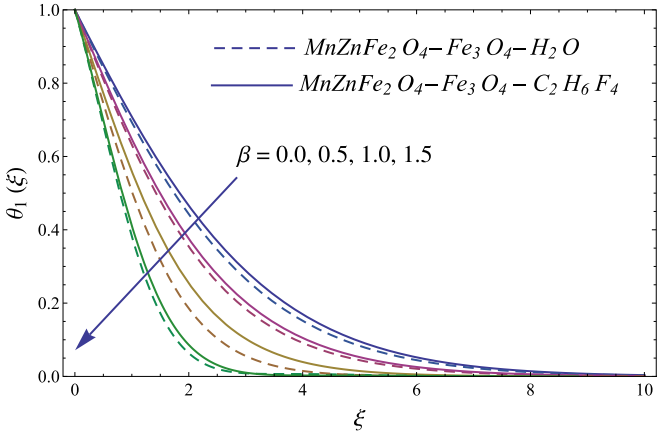

Fig. 6. Influence of β on temperature field of hybrid ferromagnetic nanofluid.

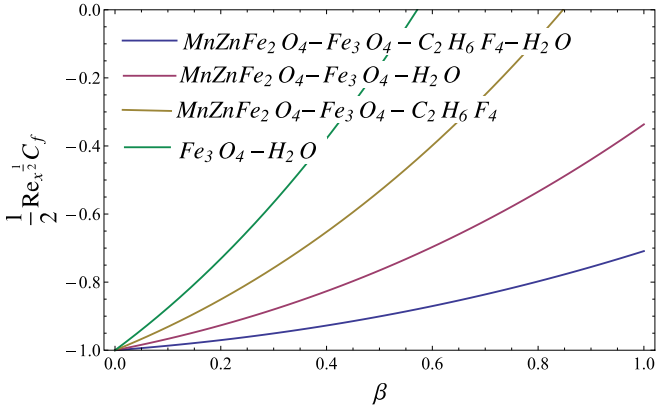

Fig. 7. Friction drag in flow of hybrid ferromagnetic nanofluid.

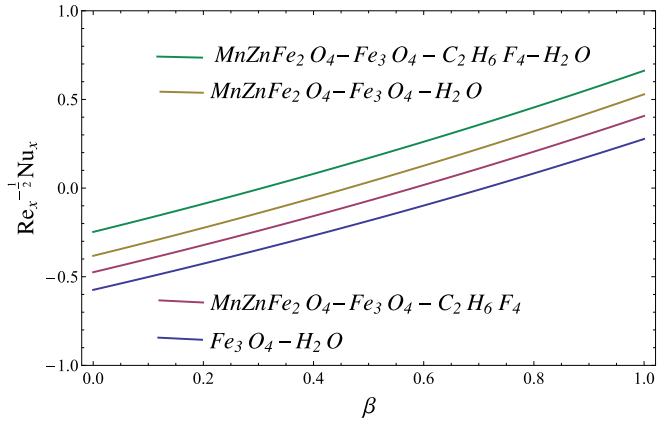

Fig. 8. Heat transfer rate in flow of hybrid ferromagnetic nanofluid.

the capability of higher velocity field as base fluid as compare to refrigerant-134A $C_2H_2F_4$. By suspending two ferrites nanoparticles in a singles base fluid i.e., Fe_3O_4 and $MnZnFe_2O_4$ in water H_2O and Fe_3O_4 and $MnZnFe_2O_4$ in refrigerant-134A $C_2H_2F_4$, then the resultant ferromagnetic hybrid nanofluids are analyzed. In Fig. 5 the higher velocity is depicted for the hybrid nanofluid made of ferrites nanoparticles Fe_3O_4 and $MnZnFe_2O_4$ in water H_2O base fluid, it is because water has higher heat capacity as compare to refrigerant-134A $C_2H_2F_4$ base fluid, thus, in Fig. 6 reduction in temperature field is demonstrated for the same hybrid nanofluids. Secondly, the variation is given to β (Ferrohydrodynamic interaction), which means that magnetization is enhanced through which more ferrites will be attracted by magnetic dipole and as a result, the velocity field enhances and temperature field declines there.

The heat transfer is analyzed employing Fourier's law. The article includes the flow of hybrid ferromagnetic nanofluids made of Fe_3O_4 and $MnZnFe_2O_4$ ferrite nanoparticles and base fluids water H_2O and refrigerant-134A $C_2H_2F_4$. The graphical results given in Figs. 7 and 8 states the friction drag and Nusselt number respectively. They are important parameters of engineering interest. Employing friction drag and Nusselt number one can decide which fluid is efficient in heat transfer. Fig. 7 depicts the friction drag or skin friction coefficient in the flow of different hybrid ferromagnetic nanofluids, i.e., $MnZnFe_2O_4$-Fe_3O_4-H_2O-$C_2H_2F_4$, Fe_3O_4-$MnZnFe_2O_4$-H_2O, $MnZnFe_2O_4$-Fe_3O_4-$C_2H_2F_4$ and a simple nanofluid Fe_3O_4-H_2O. Higher friction drag is evident for the ferromagnetic nanofluid Fe_3O_4-H_2O, whereas, the friction drag declines for the hybrid ferromagnetic nanofluids $MnZnFe_2O_4$-Fe_3O_4-H_2O-$C_2H_2F_4$. The possible reduction in fraction drag is because of the presence of distinct ferrites nanoparticles in the base fluids, these ferrites reduce the friction between fluids layers, which leads to smaller the resistance, hence friction drag declines for hybrid ferromagnetic nanofluids. On the other hand, if one looks at Fig. 8, the higher heat transfer can be seen there for the hybrid ferromagnetic nanofluid $MnZnFe_2O_4$-Fe_3O_4-H_2O-$C_2H_2F_4$, and the smallest heat transfer rate is depicted for ferromagnetic nanofluid Fe_3O_4-H_2O. Physically, when more ferrites nanoparticles are suspended in the base fluids, the resultant improve there thermophysical characteristics, which means that the resultant fluid will lead to enhance heat transfer rate, hence the hybrid ferromagnetic nanofluid $MnZnFe_2O_4$-Fe_3O_4-H_2O-$C_2H_2F_4$ results in the enhancement of heat transfer.

4. Concluding remarks

The performance of ferrites nanoparticles and their impacts on heat transfer in the flow of hybrid ferromagnetic nanofluid are scrutinized in this article. The analysis contains the suspension of two different ferrites nanoparticles in the mixture of two distinct base fluids. The resultant hybrid ferromagnetic nanofluid is studied for heat transfer. The ferrite nanoparticles Fe_3O_4 and $MnZnFe_2O_4$ are suspended in the base fluids water H_2O and refrigerant-134A $C_2H_2F_4$. The conclusion of the analysis is that hybrid ferromagnetic nanofluids $MnZnFe_2O_4$-Fe_3O_4-H_2O-$C_2H_2F_4$ is efficient in heating or cooling rates as compare to the hybrid ferromagnetic nanofluids Fe_3O_4-$MnZnFe_2O_4$-H_2O, $MnZnFe_2O_4$-Fe_3O_4-$C_2H_2F_4$ and a simple nanofluid Fe_3O_4-H_2O. The reason behind hybrid ferromagnetic nanofluid $MnZnFe_2O_4$-Fe_3O_4-H_2O-$C_2H_2F_4$ is that it contains two types of ferrites nanoparticles Fe_3O_4 and $MnZnFe_2O_4$ and two distinct types of base fluids water H_2O and refrigerant-134A $C_2H_2F_4$. These base fluids and ferrites nanoparticles have their thermophysical properties. This means that the resultant fluid has improved thermophysical properties and Curie temperature. Through which the hybrid ferromagnetic nanofluid performs well in transferring heat and reducing friction drag. Based on present analysis, it can be stated that two or more ferrites if suspended in two or more base fluids can be better for heat transfer.

Declaration of Competing Interest

We have no conflict of interest for this submission.

References

[1] R.G. Ross, P. Andersson, B. Sundqvist, G. Backstrom, Thermal conductivity of solids and liquids under pressure, Rep. Prog. Phys. 47 (10) (1984) 1347.
[2] R.C. Zeller, R.O. Pohl, Thermal conductivity and specific heat of noncrystalline solids, Phys. Rev. B 4 (6) (1971) 2029.
[3] S. Zhang, H. Zhou, H. Wang, Thermal conductive properties of solid-liquid-gas three-phase unsaturated concrete, Constr. Build. Mater. 232 (2020) 117242.
[4] R. Attri, S. Roychowdhury, K. Biswas, C.N.R. Rao, Low thermal conductivity of 2D

borocarbonitride nanosheets, J. Solid State Chem. 282 (2020) 121105.
[5] F.C. Malheiros, J. Gomes do Nascimento, A.P. Fernandes, G. Guimares, Simultaneously estimating the thermal conductivity and thermal diffusivity of a poorly conducting solid material using single surface measurements, Rev. Sci. Instrum. 91 (1) (2020) 014902.
[6] S.E. Ahmed, M.A. Mansour, A.M. Alwatban, A.M. Aly, Finite element simulation for MHD ferro-convective flow in an inclined double-lid driven L-shaped enclosure with heated corners, Alex. Eng. J. 59 (1) (2020) 217–226.
[7] A. Majeed, A. Zeeshan, M.M. Bhatti, R. Ellahi, Heat transfer in magnetite (Fe_3O_4) nanoparticles suspended in conventional fluids: refrigerant-134A ($C_2H_2F_4$), kerosene ($C_{10}H_{22}$), and water (H_2O) under the impact of dipole, Heat Transf. Res. 51 (3) (2020).
[8] N. Muhammad, S. Nadeem, M.T. Mustafa, Hybrid isothermal model for the ferrohydrodynamic chemically reactive species, Commun. Theor. Phys. 71 (4) (2019) 384.
[9] S. Nadeem, S. Ahmad, N. Muhammad, M.T. Mustafa, Chemically reactive species in the flow of a Maxwell fluid, Results Phys. 7 (2017) 2607–2613.
[10] S. Ahmad, S. Nadeem, N. Muhammad, A. Issakhov, Radiative SWCNT and MWCNT nanofluid flow of Falkner–Skan problem with double stratification, Physica A 547 (2020) 1–15, https://doi.org/10.1016/j.physa.2019.124054 124054.
[11] S. Ahmad, S. Nadeem, N. Muhammad, Boundary layer flow over a curved surface imbedded in porous medium, Commun. Theor. Phys. 71 (3) (2019) 344.
[12] S. Nadeem, A. Alblawi, N. Muhammad, I.M. Alarifi, A. Issakhov, M.T. Mustafa, A computational model for suspensions of motile micro-organisms in the flow of ferrofluid, J. Mol. Liq. 298 (2020) 112033.
[13] K.U. Rehman, Q.M. Al-Mdallal, I. Tlili, M.Y. Malik, J.N. Armstrong, S. Ren, Impact of heated triangular ribs on hydrodynamic forces in a rectangular domain with heated elliptic cylinder: finite element analysis, Int. Commun. Heat Mass. 112 (2020) 104501.
[14] Z. Abdelmalek, K.U. Rehman, N. Kousar, N. Fatima, I. Tlili, Hybrid meshed finite element analysis (HMFEM) of corrugated magnetized ongoing shear thinning/thickening liquid streams, J. Mol. Liq. 306 (2020) 112915, , https://doi.org/10.1016/j.molliq.2020.112915.
[15] K.U. Rehman, N. Kousar, W.A. Khan, N. Fatima, On fluid flow field visualization in a staggered cavity: a numerical result, Processes 8 (2) (2020) 226.
[16] K.U. Rehman, Q.M. Al-Mdallal, On partially heated circular obstacle in a channel having heated rectangular ribs: finite element outcomes, Case Stud. Therm. Eng. 18 (2020) 100597.
[17] Z. Abdelmalek, K.U. Rehman, I. Tlili, Grooved domain magnetized optimization (GDMO) of hydrodynamic forces due to purely viscous flowing liquid stream: a computational study, J. Mol. Liq. 304 (2020) 112766, , https://doi.org/10.1016/j.molliq.2020.112766.
[18] M. Nawaz, Role of hybrid nanoparticles in thermal performance of Sutterby fluid, the ethylene glycol, Physica A 537 (2020) 122447.
[19] W.K. Hussam, K. Khanafer, H.J. Salem, G.J. Sheard, Natural convection heat transfer utilizing nanofluid in a cavity with a periodic side-wall temperature in the presence of a magnetic field, Int. Commun. Heat Mass Transfer 104 (2019) 127–135.
[20] J. Prakash, D. Tripathi, O.A. Bég, Comparative study of hybrid nanofluids in microchannel slip flow induced by electroosmosis and peristalsis, Appl. Nanosci. 1 (2020) 1–14.
[21] Z.M. AL-Asady, A.H. AL-Hamdani, M.A. Hussein, Study the optical and morphology properties of zinc oxide nanoparticles, AIP Proc. Conf. 2213 (1) (2020) (020061).
[22] S. Medhi, S. Chowdhury, D.K. Gupta, A. Mazumdar, An investigation on the effects of silica and copper oxide nanoparticles on rheological and fluid loss property of drilling fluids, J. Pet. Explor. Prod. Technol. 10 (1) (2020) 91–101.
[23] M. Gupta, V. Singh, Z. Said, Heat transfer analysis using zinc ferrite/water (hybrid) nanofluids in a circular tube: an experimental investigation and development of new correlations for thermophysical and heat transfer properties, Sustain. Energy Technol. Assess. 39 (2020) 100720.
[24] M. Bououdina, C. Manoharan, Dependence of structure/morphology on electrical/magnetic properties of hydrothermally synthesised cobalt ferrite nanoparticles, J. Magn. Magn. Mater. 493 (2020) 165703.
[25] M. Kamran, M. Anis-ur-Rehman, Enhanced transport properties in Ce doped cobalt ferrites nanoparticles for resistive RAM applications, J. Alloys Compd. 1 (2020) 153583.
[26] S. Liao, Beyond Perturbation: Introduction to Homotopy Analysis Method, Chapman and Hall,CRC Press, Boca Raton, 2003.
[27] S. Liao, Homotopy Analysis Method in Non-linear Differential Equations, Springer and Higher Education Press, Heidelberg, 2012.